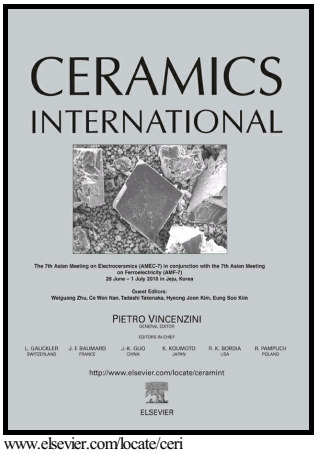

www.elsevier.com/locate/ceri

POST-MORTEM ANALYSIS OF ALUMINA-MAGNESIA-CARBON REFRACTORY BRICKS USED IN STEELMAKING LADLES

Walter A. Calvo, Pilar Pena, Analía. G. Tomba Martinez

PII: S0272-8842(18)32617-8
DOI: https://doi.org/10.1016/j.ceramint.2018.09.150
Reference: CERI19549

To appear in: *Ceramics International*

Received date: 31 July 2018
Accepted date: 14 September 2018

Cite this article as: Walter A. Calvo, Pilar Pena and Analía. G. Tomba Martinez, *POST-MORTEM* ANALYSIS OF ALUMINA-MAGNESIA-CARBON REFRACTORY BRICKS USED IN STEELMAKING LADLES, *Ceramics International,* https://doi.org/10.1016/j.ceramint.2018.09.150

POST-MORTEM ANALYSIS OF ALUMINA-MAGNESIA-CARBON REFRACTORY BRICKS USED IN STEELMAKING LADLES

Walter A. Calvo[1], Pilar Pena[2], Analía. G. Tomba Martinez[1]

[1]Instituto de Investigaciones en Ciencia y Tecnología de Materiales (INTEMA), CONICET-Facultad de Ingeniería/Universidad Nacional de Mar del Plata, Av. J.B. Justo 4302 (7600) Mar del Plata, Argentina

[2]Instituto de Cerámica y Vidrio ICV-CSIC, Kelsen 5, 28049- Madrid, España

Abstract

Post-mortem studies in secondary steelmaking ladles are an important way to determine the factors related to Alumina-Magnesia-Carbon (AMC) refractory corrosion. AMC refractory bricks installed in the impact zone of a steelmaking ladle bottom were analyzed after 100 castings. X-ray diffraction, X-ray fluorescence chemical analysis, reflected optical light microscopy, scanning electron microscopy, energy dispersive X-ray spectrometry, density and porosity measurements, and mercury porosimetry were used to analyze the chemical and physical characteristics of the slag, the unused refractory and the slag+steel attacked bricks. The corrosion process produced a specific microstructure characterized by: i) a thick discontinuous slag layer composed by secondary spinel+steel+liquid; ii) a thick dense, cracked, and continuous layer consisting of calcium aluminates+steel+liquid at the slag/refractory interface; iii) next to this layer, a wide densified layer with a uniform microstructure in which corundum aggregates and spinel crystals were linked together by elongated $CaAl_{12}O_{19}$ crystals.

The formation of these reaction layers constituted a barrier that effectively suppressed the massive slag penetration and surely reduced the wear rate. Thermodynamic calculations based on simplified and complex condensed phase equilibrium diagrams, were used to further understanding of the corrosion mechanism.

Keywords: C. Corrosion; E. Refractories; *Post-mortem* analysis

Introduction

The use of Alumina-Magnesia-Carbon bricks (Al_2O_3-MgO-C; AMC) in the bottoms and metal lines of ladles has been extended to the steelmaking industry since the 1980s. The main improvement with respect to their precursors, MgO-C and Al_2O_3-C bricks, is the decrease in joint wear due to the residual expansion originating from the *in-situ* $MgAl_2O_4$ spinel formation [1–5].

During the service of the ladle, when the secondary metallurgy takes place (i.e., the adjustment of the steel composition), refractories of the working lining are exposed to very aggressive conditions: the high temperature of the process, the oxidant atmosphere that prevails because it is an open vessel, and contact with corrosive agents, especially the liquid slag, among others. The refractories are zoned in type and thickness to provide maximum ladle performance at a minimum cost. However, the particular loading of each refractory depends not only on its location in the vessel, but also on the stage of the ladle cycle [6]: the lifetime of the refractory in the impact zone of the bottom is limited by the thermo-mechanical loading, thermal shock and erosion, which are developed during the tapping and the refining of the steel. For this reason, the use of refractories with high mechanical strength and erosion resistance at high temperatures is convenient, which is why alumina is incorporated into the refractory formulation. However this addition makes the brick incompatible with the ladle slag. Nevertheless, liquid slag is in contact with these refractories during the casting stage, giving corrosion a chance to occur before slag solidification.

This paper deals with the degradation of AMC bricks used in the impact zone of a steelmaking ladle (*post-mortem study*) with a focus on slag corrosion, bearing in mind that it undoubtedly contributed to the refractories' wear. The literature on the corrosion of AMC bricks is scarce, and the papers available concern work implemented in lab tests to the study the phenomenon [7–9]. These tests provide very helpful information, especially in terms of proposing corrosion mechanisms and

possible factors determining the corrosion behavior, but its extrapolation to the plant conditions is limited by the difficulty of reproducing the industrial conditions in the laboratory. For this reason, the evaluation of *post-mortem* materials is extremely useful for determining the wear mechanisms which take place under the real operational conditions [10]. Data collected in these types of studies increase and at the same time complement the information of those more basic works. No *post-mortem* studies of AMC bricks used in steelmaking ladle bottoms were found in the available literature.

In this paper, the characterization of fragments of AMC *post-mortem* bricks used in the impact zone of a steelmaking ladle bottom was carried out. Several analytical techniques were employed to reconstruct a possible history of the material during service, and as a result, a possible degradation mechanism. The thermodynamic simulation, a powerful tool used to study refractory materials, was performed to help in this reconstruction since lengthy exposure to the service conditions is propitious to the system (refractory/slag) evolves toward the thermodynamic equilibrium.

Materials and methods

Post-mortem (after service) AMC bricks used at the impact zone of a ladle bottom, labeled as AMC4, were provided by a local steelmaking company. Also, unused AMC4 material was available. Figure 1 shows the as-received *post-mortem* fragments of the AMC4 bricks; slag was still adhered on the hot face (working face) of bricks.

During a typical campaign, the lade furnace is vertically heated up to ~ 800°C (drying step) after the lining is assembled. Then, devices such as the porous plug and slide gate are installed, and the ladle is heated again up to temperatures of around 1100°C to 1300°C in a vertical heater (pre-heating step). When the temperature is reached, the ladle is placed in the casting car to receive the molten

steel at almost 1700°C (tapping step). Once the ladle is filled with the liquid steel, it is moved to the ladle furnace station where the temperature is maintained and the additives to adjust the slag composition and refine steel are added (secondary refining step). Later, the ladle is carried to the ladle turret of the continuous casting and placed onto the tundish. There, steel drains from the ladle bottom (casting step) until < 0.8 ton of liquid remains. After that, the ladle is taken out from the turret, and slag and steel are poured out in pots. Then, porous plugs and the slide gate/nozzle hole are cleaned, and the ladle is put in the vertical pre-heater again to reach the operation temperatures, starting a new cycle.

The *post-mortem* AMC4 bricks were remained in the ladle during a campaign of 100 castings. The steel manufactured in this plant has the following approximate composition: C = 0.08 - 0.45 wt.%, Mn = 0.6 - 1.5 wt.%, Si = 0.2 - 0.5 wt.% and Al = 0.01 - 0.04 wt.%. In the ladle, joins between the AMC bricks at the bottom were filled by a refractory mortar.

With the aim of analyzing the in-service degradation of the AMC4 refractory bricks, a thorough characterization of the unused brick was performed by means of several techniques: X-ray fluorescence (XRF), inductively coupled plasma-optical emission spectroscopy (ICP-OES), gravimetry and particle size distribution by sieving of fragments thermally treated, reflected light optical microscopy (RLOM) and scanning electron microscopy coupled with X-ray dispersive energy (SEM/EDS), X-ray diffraction (XRD), differential thermal and thermogravimetric analyses (DTA/TGA), mercury intrusion porosimetry and measurements of porosity and density, pycnometric density in He and permeability. The results of this characterization have been published on a previous work [11] and they are summarized in Table 1.

Two slices ~25 mm in thickness were cut perpendicularly to the hot face of a *post-mortem* brick (Figure 2). In addition, three cuts parallel to the hot face were made in each slice to obtain four

samples with ~ 20 mm of thickness. These prismatic samples (20x20x25 mm^3) were labeled as PM1, PM2, PM3 and PM4, and are representative of the brick at different distances from the hot face, as shown in Figure 2 (PM1 contains the hot face and the adhered slag). The samples were obtained by cutting and machining using diamond disks and drills.

Several techniques were used to analyze *post-mortem* specimens (PM1 to PM4) in order to evaluate the in-service refractory degradation. Powdered samples were obtained by milling in a planetary mill (Planetary-Micro Mill "Pulverisette 7", Fritsch) at 595 rpm, and manual milling with tungsten mortar.

The mineralogical qualitative analysis of *post-mortem* specimens was carried out by X-ray diffraction (DRX; Panalytical X´PERT PRO) on powdered samples (< 75 μm), using Cu Kα radiation at 40 kV and 40 mA, at a rate of 1°/min. Thermal gravimetric analysis (Shimadzu TGA 50) of samples powders (< 75 μm) up to 1200ºC, using a heating rate of 10ºC/min in air, was also performed. The pycnometric density of the solids (ρ_{pyc}) was determined using kerosene as fluid at 37°C. The global density (ρ_g) and the apparent porosity (π_a) of *post-mortem* specimens were determined using the Archimedes method based on DIN EN 993-1 (DIN 51056) standard [12] using kerosene. The close (π_c) and true (π_t) porosities were calculated using the following equations:

$$\pi_t = \frac{\left(\rho_{pyc} - \rho_b\right) \times 100}{\rho_{pyc}}$$

$$\pi_c = \pi_t - \pi_a$$

The microstructures of the corroded (PM5, Figure 2) and unused AMC4 bricks were characterized using reflected-light optical microscopy (RLOM; Model HP 1, Carl Zeiss, Oberköchen and Jena) on polished surfaces of the specimens. The microstructure of these sections was also studied

using a field emission scanning electron microscope with X-ray energy-dispersive spectrometric microanalysis module (FE-SEM-EDS; S-4700, Hitachi). Before that, the samples were impregnated in polyester resin in vacuum and polished using SiC papers up to 4000 grit. For the final polishing, diamond pastes up to 1 µm were used. Polished surfaces coated with Au were analysed.

The composition of the ladle slag in the middle of the last casting where the AMC4 refractories were used, labeled as m-slag, was determined by X-Ray fluorescence (XRF; Thermo Electron ARL model 9900). In addition, the slag adhered in the hot-face of the *post-mortem* bricks, designated as a-slag, was analyzed by XRF and XRD under the same conditions as those used for the other slag and the *post-mortem* samples, respectively. This slag was easily detached from the *post-mortem* brick as fine dust. The viscosities of both slags were calculated using the Urbain model [13] which takes into account the slag composition (in oxides) and the temperature. The softening, hemisphere and fluidity temperatures of the a-slag were obtained by hot stage optical microscopy using a lab-made equipment.

The thermodynamic simulation of the evolution of the unused AMC4 refractory in the temperature range between the pre-heating temperature up to 1700°C was performed taking into account the fact that the ladle refractory lining undergoes thermal treatments repeatedly, which favors the bricks reaching thermodynamic equilibrium. Furthermore, the contact refractory-slag was simulated at the most critical temperature during service, using a corrosion modeling proposed in previous works by the authors [14,15]. The evolution of the m-slag during cooling was also analyzed. The calculations were carried out using FactSage 7.0 and the Equilib Module, based on the minimization of the free energy of the system in order to determine the nature of each phase as well as their proportion at a given pressure and temperature.

The chemical compositions of the unused AMC4 brick (Table 1) and that of the m-slag (Table 2) was taken into account to simulate the corrosion process. The resin content of the refractory was dismissed since the databases do not have information pertaining to organic compounds. An iterative process previously used for similar systems [14] was employed. First, 100 g of refractory

and 100 g of slag were considered in the first reaction stage. The resulting liquid was again put in contact with 100 g of the previously used original refractory composition used before and another calculation step was carried out. This procedure was repeated (calculation steps, CS) until no liquid was present in equilibrium state of the system. All calculations were performed at 1700ºC and at 1 atm of pressure.

Results and discussion

In Figure 3a, the aspect of the PM5 sample containing the slag-refractory interface can be observed. Compared to the characteristics of the unused AMC4 brick (Figure 3b), the wear and the decarburization of the used material are visually detected, especially on the hot face. The original dimensions of the brick were 10x15x25 cm^3 and the working face was that of 10x15 cm^2 in area. The length of *post-mortem* fragments was ~11 cm, which represents a wear of approximately 56 % after 100 castings.

A region ~0.7 cm in depth from the hot face where slag and metal infiltration took place is evident; this region is characterized by a strong change in the brick's texture. Two different zones are distinguished in this region: a working zone with a color different to that of the unused brick, which reveals the contact with the slag and decarburization, and a second zone of extended corrosion where steel infiltration and the formation of fissures and pores are observed. Far away from the slag-refractory interface, the material shows little alteration. Only a discoloration of the original brown aggregates was detected; this phenomenon, which is likely related to the sintered magnesia or brown fused alumina particles, is attributed to the oxidation and/or migration of impurities responsible for this color (Fe^{+2}, Ti^{+2}) during the brick 's time at the high temperature of ladle operation.

The composition of both analyzed slags, that of the middle of the last cycle (m-slag) and that adhered to the *post-mortem* bricks (a-slag), are shown in Table 2. The first slag corresponds approximately to that which was in contact with the AMC4 bricks when the ladle was emptied the last time. On the other hand, the a-slag is roughly that which was formed by cooling of the remnant liquid after the attack to the brick. For this reason, the latter has a higher amount of alumina (~ 25 % higher) due to the corrosion to the AMC refractories formed mainly by Al_2O_3. This is also the cause of its higher viscosity (μ) calculated with the Urbain model (Table 1); this increase could have discouraged the slag penetration as it interacted with the refractory, and as a consequence, contributed to stopping the corrosion. Moreover, the a-slag has a higher content of FeO with respect to m-slag; this is probably due to the mixing of the molten metal with the liquid slag during ladle operation. The softening temperature of the m-slag calculated as the temperature of the first liquid formation using FactSage software was 1256ºC. When this value was exceeded, the slag would be in a condition to penetrate the refractory. Furthermore, the softening temperature of the adhered slag determined by hot microscopy was higher due the change in composition: 1369ºC±5°C.

The equilibrium phases during the evolution of the AMC4 brick in the thermal range to which it was exposed in service, from the initial pre-heating to the tapping temperature, are shown in Table 3. Since the brick was not directly exposed to air (only the external surface was in contact with the atmosphere during pre-heating), no additional oxygen (as O_2) was added in the simulation. These solids are those expected to be found in the PM1 to PM4 samples if the equilibrium condition was reached after the 100 castings. On the other hand, equilibrium phases formed during m-slag cooling are reported in Table 4; these solids are comparable to those present in the adhered slag. Finally, the evolution of condensed main phases present in the equilibrium of the refractory-slag system at the most critical condition are shown in Figure 4, as a function of the calculation step (CS). The

composition of these phases is also indicated, as well as the variation of liquid viscosity calculated with the Urbain model (Figure 4c).

According to the information in Table 3, the most significant transformations between the refractory's components had already taken place at 700°C: without excess of O_2, Al and Si react with graphite to form carbides, and magnesia with alumina to form MA ($MgO{\cdot}Al_2O_3$) spinel. The increase in the proportion of the latter, which occurred simultaneously with the reduction in the amount of Al_2O_3, is due to its incorporation into the spinel structure as a solid solution. It is known that, due to kinetic factors among others, these transformations occurs just over 1000°C in the real material. However, the equilibrium condition serves as a guide to understanding the changes taking place inside the refractory brick as the temperature increases, especially after a high number of castings, such as in this case.

The crystalline phases identified in diffractograms of *post-mortem* samples are provided in Table 5.

In agreement to that shown in the thermodynamic simulation, spinel (MA) was detected in every specimen; moreover, Al peaks disappear in all of PM samples, and those of magnesia only in PM1 and PM2. The intensities of the spinel XRD peaks were similar in the four specimens. The absence of Al_4C_3, which was predicted as an equilibrium phase, is attributed to the fact that this solid decomposes quickly when oxidant agents are present, or it reacts with MgO to form spinel, as was determined in the thermal evolution in air of unused AMC4 [11]. Likely, the brick had been exposed to a more oxidant condition during service than that simulated in the equilibrium calculation.

The disappearance of metallic silicon XRD peaks was observed in all of the *post-mortem* specimen diffractograms, in agreement with the tendency marked by thermodynamics (Table 3), although no other Si-containing phases could be identified using this technique, such as SiC for instance, which should be present in the equilibrium state. However, this last solid was actually detected when unused AMC4 was thermally treated at 1600°C. On the other hand, mullite formation was observed when unused AMC4 was heated up to 1400°C in air even though no indication of the presence of carbide was identified in this case. According to that reported by Taffin and Poirier [16], incipient formation of SiC takes place at 1100°C by reaction of the SiO_2 formed in the Si particle's surfaces; the metal reacts completely at 1300°C. According to these authors, there are also volatilization processes which lead to further condensation of gaseous species in the form of glassy silica into pores. The occurrence of these processes could justify the absence of SiC in *post-mortem* specimens (or its presence in an amount lower than the sensitivity of the technique), indicating that the temperature in the cold face was higher than 1300°C during service. It is possible that this occurred during the last castings of the ladle, when the brick length was reduced considerably. Furthermore, the SiO_2 formed in the working face by the oxidation of Si and intermediate SiC, would be dissolved in the liquid slag.

According to the data in Table 5, graphite persisted in all of the *post-mortem* samples, in line with that established by the thermodynamic simulation (Table 3). However, in contrast with the decrease in the initial content of this component du supposedly to its reaction with Al and Si to form carbides, the main diffraction peak of graphite in PM1 to PM4 exhibited intensities similar to that of the unused material. This disagreement may have at least two causes. On one hand, the residual carbon coming from the resin pyrolysis is the most reactive, but it was not assessed in the thermodynamic simulation. On the other hand, the presence of Si in AMC4 strengthens its resistance to oxidation, especially in the range of high temperatures [11], which could be another reason for the persistence of graphite in *post-mortem* specimens.

In order to collect more evidence concerning this issue, TGA of *post-mortem* and unused AMC4 materials were obtained, as shown in the curves of Figure 5. As has been previously reported for unused AMC4 [11], the mass losses between 300 and 500ºC are attributed to the elimination of resin volatiles, and those between 600 and 800ºC, to graphite and residual carbon oxidation.

No losses between 300 and 500°C were displayed in *post-mortem* specimens due to the pyrolysis of resin occurred during service, probably during the pre-heating before the first cycle of the ladle. Nevertheless, mass losses corresponding to carbon oxidation (between 500 and 800ºC) were observed; these values are shown in Table 6.

PM1 showed a mass loss between 500 and 800ºC that was lower than that of the other *post-mortem* samples due to the greater decarburization undergone by the working face (as can be observed in Figure 3), which was exposed directly to the atmosphere (in the last pre-heating) and the highest temperatures. It draws attention to the fact that the mass losses corresponding to the carbon oxidation for PM2, PM3 and PM4 are higher than that of the unused material, indicating that the carbon content not only maintained its original level, as suggested by the XRD analysis (Table 5), but also increased during service. This fact was confirmed in the thermal treatment up to 500 and 800°C simulating the TGA schedule, of samples of the *post-mortem* and unused materials of greater mass (3.5 g). Moreover, additional XRD analyses at a slower rate (º0.125/min) of the unused and *post-mortem* samples, in the º2θ range where a diffraction peak of corundum at 25.50 º2θ (75 % I/I_0) and the main diffraction peak of graphite at 26.28 º2θ were positioned. From the comparison of

the area under these peaks, it was confirmed that the intensity of the graphite peak did not show a significant reduction in PM2, PM3 and PM4 with respect to the unused material.

However, the question is how the increase in the carbon content shown in thermograms of Figure 6 could have taken place during service? A plausible explanation would be that the thermal gradient generated in the brick during the steelmaking process, from ~1700ºC in the hot face to lower temperatures at the opposite face (near 1300°C in the last castings), causes the CO_2 and CO produced by resin pyrolysis, the reaction of residual carbon, and the oxidation of graphite (which should occur at least during pre-heating), to move from the hot face toward the cold face due to the lower pressure in this region (caused by the lower temperature). Gases such as CO_2 and CO may react with MgO and/or Al_2O_3, generating reaction products of low crystallinity, such as carbides, oxycarbides and amorphous carbon (soot), which are not easily detected by XRD. Some of these reactions, which imply an increase in the carbon content, are the following:

$$CO_{(g)} \rightarrow C_{(s)} + ½\ O_{2(g)}$$

$$CO_{2(g)} \rightarrow C_{(s)} + O_{2(g)}$$

$$MgO_{(s)} + 2\ Al_{(l)} + 3\ CO_{(g)} \rightarrow MgO{\cdot}Al_2O_{3(s)} + 3\ C_{(s)}$$

$$Al_4C_{3(s)} + 2\ MgO_{(s)} + 6\ CO_{(g)} \rightarrow 2\ MgO{\cdot}Al_2O_{3(s)} + 9\ C_{(s)}$$

$$Al_4C_{3(s)} + 6\ CO_{(g)} \rightarrow 2\ Al_2O_{3(s)} + 9\ C_{(s)}$$

$$Al_{(g)} + Mg_{(g)} + 4\ CO_{(g)} \rightarrow MgO{\cdot}Al_2O_{3(s)} + 4\ C_{(s)}$$

Support of this hypothesis comes from the fact that the onset of the mass loss, as well as the minimum in TGA curves around 800°C, shifted to lower temperatures in the *post-mortem* samples with respect to the original AMC4 material; this signifies that the generated carbon is more reactive than the original carbon. Assuming that the evolution of CO/CO_2 produced is greater in the hot face and that the migration of these gases should be toward the opposite face, a maximum concentration

of carbon should be present inside the brick. According to thermograms, this maximum is located in PM2, whose center was approximately 3 cm from the last hot face.

In *post-mortem* samples farther away from the working face, where the temperature was lower, not all magnesia was converted to spinel (Table 5), as would occur under equilibrium conditions (Table 3). In previous work by the authors [11], it was found that the degree to which spinel formation advanced was lower in AMC4 than in other AMC refractories with a similar MgO content, which was attributed to the larger size of the magnesia particles. Taking into account that the amount of spinel formed during service was similar along the brick length (Table 5), the absence of periclase in *post-mortem* specimens near the working face was not likely produced by a higher conversion to spinel, but by the consumption of MgO in another process. Due to the high temperature in this region (~ 1700°C), the reactivity of solids is rather high. For instance, magnesia could react with carbon by the carbothermal reduction in the hotter zones (PM1 and PM2) according to: $2\ MgO_{(s)} + C_{(s)} \rightarrow CO_{2(g)} + 2\ Mg_{(g)}$ [17–19] due to thermal conditions (T >1200ºC) plus a low oxygen partial pressure. The $Mg_{(g)}$ probably escaped from the brick without re-oxidation or, if this oxidation took place, the new MgO was dissolved in the slag. This process could explain the absence of MgO in the samples near the working face without a simultaneous increase of the spinel proportion in this region.

In the XRD diffractogram analysis of the adhered slag, the following crystalline phases were identified (ICDD files in parenthesis), in agreement with the high content of Al_2O_3 characteristic of Al-killed steel refining [20], and its ternary basicity index [21]: $C_{12}A_7$ ($12CaO{\cdot}7Al_2O_3$; 00-009-0413), C_3A ($3CaO{\cdot}Al_2O_3$; 00-001-1060), CA_2 ($CaO{\cdot}2Al_2O_3$; 00-023-1037), MA ($MgO{\cdot}Al_2O_3$; 00-034-0189), CaO (01-075-0264), C_2S ($2CaO{\cdot}SiO_2$; 00-001-1012), FeS_2 (00-003-0822), $Ca(OH)_2$ (00-044-1481), $Mg(OH)_2$ (00-044-1482), MgO (00-045-0946). Mayenite ($C_{12}A_7$) and celite (C_3A) were identified as major phases. The coincidence shown with the mineralogical composition of the equilibrium states of m-salg in the temperature range up until its solidification (Table 4) is rather high. On the other hand, the identification of Ca and Mg hydroxides in the a-slag is due to its

hydration caused by the presence of free lime (CaO) and free magnesia (MgO) as equilibrium phases (formed at high temperature and detected by XRD), which are readily attacked by humidity [20,22]. This is the reason why this slag detached easily from the hot face, since these hydrations have significant associated volumetric variations, that lead to fragmentation [22,23]. This is also the cause of the slight increase of mass displayed in the thermogram of PM1 over 100°C (Figure 5), due to the dehydration of the hydrates present in the a-slag.

The information contained in the plots in Figure 4 helps to understand the interaction between the slag and the AMC4 refractory during successive cycles in service, which could be the origin, although not exclusively, of their degradation. The number of calculation steps (CS) required for corrosion to stop has been considered as indicative of the material's corrosion resistance [14,15]. Taking this into account, high corrosion wear is expected to occur under service conditions for AMC4 bricks if this parameter (CS=12) is compared with those resulting from the simulation of the corrosion of other AMC refractories with similar MgO content at 1600°C (CS=3 or 4) is done [14]. Experimental corrosion wear for these AMC refractories in lab testing was ~10 % [14].

As can be observed in Figure 4a, the liquid percentage in the first CS is very high, dissolving the refractory's components almost completely; as a result, a severe attack of the refractory by the molten slag at ~1700°C when the ladle was empty should be expected. In Figure 4c, the variation in the liquid viscosity with increasing CS is shown; the value for CS=0 corresponds to the viscosity of the m-slag at 1700°C (Table 2). After an initial increase due to an increase in Al_2O_3 content (from ~ 27 wt.% to ~60 wt.% in the first CS, Figure 4b) and a decrease in the Fe^{+2}/Fe^{+3} content (< 10^{-3} wt.%, Figure 4b), the viscosity value decreases, with a tendency towards to 2,18 poise, higher than the value at the beginning. This behavior implies that as that slag penetrated into the refractory, its aggressiveness decreased, contributing to stopping corrosion.

As a product of the liquid saturation in Mg and Al, the thermodynamic simulation predicts the crystallization of $MgAl_2O_4$ first, and then (CS = 4) CA_6. From the fourth calculation step onwards,

the proportion of the liquid's major components remain constant. The amount of CA_6 increases in subsequent steps, until corundum becomes a stable phase towards the end of the process.

According to the data in Table 5, the solid formed by the interaction slag-refractory (ICDD files between parenthesis) were only identified in PM1: calcium aluminates CA (00-034-0440), CA_2 (00-023-1037) and CA_6 (00-025-0122). Among these phases, only the latter would be formed during the attack of the slag at the maximum operation temperature (~1700°C), according to the results of thermodynamic simulation. In addition, MA spinel was detected in PM1, which could be formed by reactions of the refractory components, or by the brick's reaction with the slag, according to Figure 4a. A more detailed picture of the slag-refractory interface was obtained by microscopic observation of the extended corrosion zone (PM5). The microstructural study by RLOM and SEM-EDS of the steel+slag reaction area put in evidence the formation of various reaction layers at the steel+slag/refractory interface (Figures 6-8):

a) *Slag zone*: a discontinuous layer with a thickness of ~200 μm formed by a calcium aluminate rich liquid phase with small amounts of cubic particles of $[(Mg,Fe,Mn)(Al,Cr,Fe)_2O_4]$ spinel and steel (see Figure 6a).

b) *Reaction zone*, composed by two layers:

- a continuous dense layer ~ 500 μm in thickness of (Figure 6a); a smooth region is present which likely corresponds to CA_2+liquid, in agreement with the observations of other authors [7,24–26] and XRD data (Figure 6b). SEM/EDS analysis of the attacked zone of the *post-mortem* brick (Figure 7, PM5) confirmed the presence of the reaction products detected by XRD (in PM1) and optical microscopy. The average composition of this layer as determined by energy dispersive X-ray microanalysis was approximately: 64 wt.% Al_2O_3, 18 wt.% CaO, 7 wt.% Fe_2O_3, 6 wt.% SiO_2, 4 wt.% TiO_2 and 1.4 wt.% MnO (Figure 7a). This composition is compatible with the presence of

calcium aluminates (CA_2), steel and amorphous phases (Figures 6b, 7c and 8). The calcium aluminate can be formed by the reaction of the molten slag with the corundum particles present in the original brick: Al_2O_3+Liq→CA_2. In the less textured region, some EDS points compatible with CA_2 and CA_2S (anorthite) were identified; points with CA composition were also detected.

- deeper into the refractory, a wide and porous layer composed by elongated crystals (~ 30 um in length and 3 um in width) but with angular pores, which can be associated with calcium hexaluminate crystals (SEM–EDS analysis: ~ 86 wt% Al_2O_3 ~ 9 wt.% CaO, and ~ 4 wt.% TiO_2 and/or SiO_2). Unreacted corundum aggregates and steel, with some spinel rich areas (probably associated with the periclase grains present in the original brick; MgO+Liq→$MgAl_2O_4$) were also observed (see Figure 7). This area is characterized by a completely reacted matrix which still retains the texture and composition of the largest aggregates of corundum (Figure 7). Typical needle-like crystals of CA_6 surround alumina aggregates that were not completely attacked; this calcium aluminate may be formed by reaction of the molten slag with corundum [7,15,24–26]: Al_2O_3+Liq→CA_6, or via the calcium dialuminate: CA_2+Liq→CA_6.

The fact that some coarser alumina aggregates maintained their integrity can be associated with the formation of this CA_6 layer (indirect corrosion) that interposes itself between the refractory particles and the liquid slag [27]. After that, corrosion probably becomes a diffusion controlled process; it is expected that this change leads to a deceleration of corrosion.

The CA_2 identified in the reaction zone is not a stable phase at 1700ºC according to the thermodynamic simulation as it was performed (Figure 4). However, the corrosion mechanisms can also be discussed graphically in terms of the involved phase equilibrium diagrams in order to explain how the calcium dialuminate appeared in the final microstructure of the corroded *post-*

mortem brick. The AMC4 refractory belongs to the Al_2O_3-MgO-SiO_2-C quaternary system, and when it reacts to the slag, other components such as CaO and Fe should also be considered as constituting a diagram with 6 components. However, taking into account the main components of the whole system, the reaction between the refractory and the slag can be studied in terms of the Al_2O_3–MgO–CaO condensed phase diagram. In Figure 9 is present the isothermal section for 1650ºC, a temperature somewhat lower than the maximum of the processing.

During the corrosion process, the slag penetrates the refractory through the open pores and grain boundaries, and the slag near the hot face dissolves the refractory and gradually changes its composition moving from the point corresponding to the m-slag simplified composition toward the AMC4 simplified composition in Figure 9. This produces the partial dissolution of alumina (Al_2O_3), magnesia (MgO) and spinel ($MgAl_2O_4$) particles of the refractory, and the precipitation of MA, CA_2 and CA_6 crystals at the refractory/slag interface (as was actually observed by microstructural analysis, Figures 6 to 8). Considering this result, the formation of CA_2 crystals could be produced during cooling stage.

Furthermore, let's consider the heterogeneity of the refractory which causes local variations of the composition. R1 and R2 points in Figure 9 represent zones of AMC4 with different MgO content, such as an alumina aggregate and a matrix region with small particles of alumina and magnesia, respectively. Considering the connecting line between the slag and each of the refractory compositions, the reaction path initially passes through the primary fields of CA_2 (for R1) or MA (for R2). Refractory zones with higher magnesium content will cause the intersection point on the liquidus line to occur below the calcium dialuminate field (see Figure 9). Therefore, the primary CA_2 or MA crystals start to precipitated at intersection point X and Y, respectively (see Figure 6a). After the primary crystals formation, the crystallization of the secondary phase (MA or CA_2) takes

place. Finally, the formation of CA_6 occurs. This aspect of the slag-AMC4 contact cannot be taken into account in the thermodynamic simulation as it was performed because it considered the global chemical compositions of the slag and the refractory.

The formation of CA_2 and CA_6 phases causes CaO to gradually decrease in the composition of the liquid phase, increasing its viscosity. At this point, the corrosion process towards the interior of the refractory is caused by diffusion of a less aggressive melt depleted in Ca. This melt is rapidly saturated in alumina, thus resulting in the formation of CA_6 and more MA. The phases present at the slag interface (MAss+liq; liquid+CA_2+MA; CA_6+MA+A) are those expected according to the proposed phase equilibrium diagram in the Al_2O_3 rich-region (Figure 9).

From the thermodynamic calculation as well as from the analysis in the paragraphs above, MA spinel is the first stable solid formed at 1700ºC; moreover, this solid is actually a solid solution that contains excess of Al^{+3} ions and small amount of iron ($Fe^{+2/+3}$). MA spinel was also identified by SEM/EDS in the extended corrosion zone, with different ions in solid solution (Mn^{+2}, Fe^{+2}, Ti^{+4}, Al^{+3}). As is already known, the cubic crystalline structure hosts cations [27]; it thus favors the increase of melt viscosity in the case of iron catchment. Even though it was not possible to confirm the origin of the spinel crystals identified by SEM/EDS, since they may be also formed *in situ* by the reaction of the refractory's own components, it is more likely that it corresponds to that crystallized by the saturation of slag in MgO (primary or secondary spinel, Figure 9). The *in situ* spinel formed over 1000°C is usually fine-grained and, as a consequence, easily dissolved by the slag [14].

In contrast with corundum aggregates which were identified in a partially attacked state in the reaction zone (Figure 7), no MgO particles were observed, which is in line with that predicted by the thermodynamic simulation since it is not an equilibrium phase. According to these data, the periclase in contact with the slag was strongly corroded by this liquid, inducing its complete dissolution.

The CA identified in the reaction zone is not a stable phase at 1700ºC according to the thermodynamic simulation as it was performed (Figure 4) nor it is based in the analysis of phase diagram (Figure 9). It is possible that this phase formed during cooling in a region where slag was concentrated, taking into account that this solids can be an equilibrium phases for the slag composition (Table 4). Furthermore, a fact which cannot be dismissed is that the simulation considers all the components of the refractory available to be dissolved, when actually only the finest particles in the matrix will dissolve first or more easily, and aggregates will react partially, as the attacked particles of alumina dispersed in the reaction zone show. Finally, the restriction in the mobility of species (kinetic factor) most certainly played an important role in determining the characteristics of the final interface microstructure.

It must be kept in mind that the infiltration of steel was observed in the hot face of *post-mortem* fragments (Figure 3 and 6), the contact between the refractory AMC4 and the molten steel (without the incorporation of additional O_2, and with the average content of C in the steel) was also simulated. As a result, only the reactions between the own components of the refractory and the metallurgy transformation of iron to form cementite take place. It was concluded that the contribution of the steel to the brick wear was due to mechanisms other than chemical attack, such as physical and/or mechanical effects.

Molten steel may cause damage to the refractory brick through its contribution to crack formation, as was observed in the extended reaction zones (Figure 1). As described above, the ladle was pre-heated between 1100ºC and 1300°C before it received the steel. At these temperatures under air, transformations in the material includes an increase in open porosity as a consequence, as is observed in Figure 10 for AMC4 samples treated at different temperatures in PLC tests [11]. Distribution of pores sizes < 10 μm for the last cycle of PLC tests (3 or 5 cycles) is shown in Table 7.

The greater change in porosity occurred after the first heating cycle, reaching similar values between 1000 and 1400°C (in this last condition, there is evidence of sintering of the finest particles). This behavior was also observed in service, as indicated in the apparent porosity variation of *post-mortem* samples; porosity values are reported in Table 5 and plotted in Figure 7 for comparison (previously corrected for the difference in the fluids used for determinations, alcohol or kerosene). According to these data, the porosity of AMC4 bricks would increase during the first pre-heating in function of the distance to the hot face; after that, the rate of change in the open pores volume probably decreased.

The data in Table 7 show that the increase in apparent porosity (in PLC specimens) was accompanied by the joining of smaller pores to generate larger pores, producing a shift of the pores sizes distribution to larger values; this was also observed in the complete pore size distribution including pores > 10 μm. It was expected that a similar process occurred in the AMC4 bricks during service, along with a decrease in the closed pore volume recorded near the hot face (Table 6), due to the opening of this type of pores. All these changes in porosity (increase in volume and size of pores, closed pores opening) are associated mainly with volatile elimination during the first steps of resin pyrolysis (which occurred during the first heating of the ladle from ~300°C), and the volatilization of different species, more than with the oxidation of carbon previously discussed. Together with these changes in porosity, a reduction in the load bearing capacity takes place in this type of AMC brick [14]. For this reason, when the brick is impacted by the steel jet the first time, the liquid can penetrate it through the open pores and cracks already present, and even create new ones which certainly detach brick fragments (erosion). This is the most critical condition of the bricks in the impact zone of the ladle bottom: the impact of the steel, a sudden thermal change (thermal shock) and erosion. Furthermore, the steel drops, along with the whole system, expand and shrink differentially as consequence of the thermal changes during the ladle cycles. Taking into account the thermal expansion coefficients of the main components of AMC4 after the first castings

in which the main transformations take place along the brick (most of them irreversible in nature), that of steel is somewhat higher: ~ $11x10^{-6}$ °C^{-1} compared to $7.4x10^{-6}$ °C^{-1} for alumina, $8.8x10^{-6}$°C^{-1} for spinel and $7.8x10°C^{-6}$ °C^{-1} for polycrystalline graphite. For this reason, expansion-contraction cycles throughout service will encourage cracking, and thus higher steel or slag infiltration at the end of the ladle campaign.

Another process related to cracking in the refractory itself, and which is independent of the steel infiltration, is spinel formation [1,3,28–31]. When slag is present, the crystallization of acicular CA_6 with anisotropy expansion properties, especially if assisted by a melt [25] as in this case, is another source of crack formation [24,32].

The pores size distribution shown in Table 7 corresponds to those pores playing an important role in slag penetration [11]. The increase in the medium pore diameter due to the temperature effect would favor slag penetration according to the following equation [27]:

$$dl/dt = r^2 \Delta P/(8\eta l)$$

where *dl/dt* is the slag penetration rate through pores (considered as capillaries), *l* is the depth of slag penetration *r* is the pore radius, ΔP is the capillary suction (which increases as pore size decreases) and η is the slag viscosity. The hot face, at a higher temperature, is most prone to be infiltrated; toward the brick's inner region, this tendency decreases as temperature and pore size are reduced.

Degradation mechanisms in AMC bricks by aluminate calcium slags

The AMC brick in the impact zone of the ladle bottom suffered serious damage during the campaign, losing approximately half of its initial volume. According to the analysis of results obtained in this work, the following degradation mechanism during service is proposed:

1) *Volatile elimination, porosity increase and decarburization*

- In the pre-heating before the first ladle cycle, the refractory lining was in direct contact with the ambient atmosphere at a temperature of around 800-1300°C. At this stage, significant changes begin to occur involving the entire brick structure, especially the resin pyrolysis (beginning at ~300°C), which leads to an increase in the open porosity volume as well as pore sizes, more marked in those hotter zones near the working face. As result, the layers closer to the surface of the bricks become mechanically weaker.
- During the wait, other chemical and mineralogical changes happen within the refractory brick, especially those involving Al, Si and MgO; some of these contribute to enhancing the mechanical properties of the bricks [33], although they may also contribute to increased porosity volume [34]. In spite of the oxidant atmosphere, the loss of graphite and/or residual carbon does not seem to contribute to refractory degradation in a significant way.

2) *Infiltration of molten steel through the open pores*

- The bricks receive the liquid steel jet at a temperature near 1700ºC at the first time; in this process, refractories undergo thermo-mechanical loading by impact, thermal shock and erosion. As a consequence, the material of the outer and weaker layers is lost. In this condition, the molten steel penetrates the bricks through open pores and cracks, and may also open new ones; therefore, heating and cooling cycles may promote damage by differential volume changes.

3) *Infiltration of the molten slag through the open pores and grain boundaries with the formation of reaction layers*

- Liquid slag floating over steel comes into contact with the refractories just at the end of the ladle cycle, when the steel is casted to the tundish. There is evidence that the slag penetrates the AMC4 refractories and attacks the most susceptible matrix, including the coarser particles, dissolving them partially (such is the case with corundum aggregates) or completely (periclase and finer corundum particles).

- During the corrosion process, the liquid slag (rich in calcium aluminates) reacts with the major components of the refractory (Al, Mg) causing the formation of various reaction layers: a) a thick discontinuous layer formed by small amounts of spinel [$(Mg,Fe,Mn)(Al,Cr)_2O_4$] grains + steel + liq at the molten slag/refractory interface, b) a dense zone formed by CA_2 + MA + steel + liq and c) a wide porous area formed by crystals of CA_6 that forms a dense network between unreacted corundum aggregates and spinel grains, which contributes to diminishing the advance of corrosion.
- The formation of this layer may constitute a barrier which effectively suppressed massive slag penetration into the decarburized refractory zone. For other reasons such as slag viscosity increase, its saturation and finally, its solidification, this process may also stop. Hexaluminate formation (which seems occur extensively) may also cause mechanical damage to the outermost layers.
- The ladle stays waiting for a new steel charge while maintained at high temperature (< 1300°C). Due to the material loss, the length of the bricks is reduced and the thermal gradient between the hot and cold faces becomes steeper; according to the results of this paper, the bricks' length decreases to 56 % of their original size, and the temperature at the cold face may reach approximately 1300°C.

Conclusions

The main factors responsible for the degradation of AMC bricks used at the impact zone of a steelmaking ladle bottom could be identified by a *post-mortem* analysis, with a focus on slag corrosion wear. A detailed characterization of the unused AMC brick served as a reference to detect the changes which took place in the refractory during service, thanks to a complete evaluation of the *post-mortem* material. The use of thermodynamic tools contributes to understanding the chemical interactions between refractory's components when the ladle is heated the first time onwards, and between the bricks and the liquid slag when they come into contact at the end of each cycle.

Considering all the obtained information, a possible degradation mechanism was proposed for the AMC studied bricks. The main processes which lead to refractory wear are considered to be:

*the increase in open pore volume and size due to volatile elimination mainly during resin pyrolysis in the pre-heating stages;

*contact with the steel jet, which produces mechanical impact, thermal shock and erosion;

*liquid steel infiltration, which causes mechanical damage, i.e., cracking;

*contact with the molten slag at the end of casting.

As a consequence of the repeated actions of all of these processes over the lifetime of the AMC bricks studied in this work (100 castings), thickness was reduced by more than a half of the original value.

It was determined that the liquid slag penetrates the AMC bricks and actually attacks the refractory components. In consequence, the refractory matrix and part of the finer aggregates, mainly those of periclase, dissolve in the liquid. In addition, solids such as $MgAl_2O_4$ (with ions in solid solution), CA_2 and CA_6 crystallize; the layered morphology of the last phase could act as a corrosion barrier. Other processes, such as the increase in slag viscosity, also contribute to stopping slag corrosion.

Acknowledgments

This work was supported by the Agencia Nacional de Promoción Científica y Tecnológica (ANPCyT) of Argentina under project “Degradación química de refractarios de uso siderúrgico”, PICT2012 N°1215. The authors would like to thank Dr. P.G. Galliano for providing the material and participating in useful discussions, and Dra. E. Brandaleze for the opportunity to use the FactSage software.

Declarations of interest:

none

References

[1] A. Watanabe, H. Takahashi, S. Takanaga, N. Goto, O. Matsuura, S. Yoshida, Thermal and Mechanical Properties of Al_2O_3-MgO-C Bricks, Taikabutsu Overseas. 10 (1990) 137–141.

[2] A.D. Gupta, K. Vikram, Development of Resin-Bonded Alumina-Magnesia-Carbon Bricks for Steel ladle Applications, Interceram. 48 (1999) 307–310.

[3] M. Kamiide, S. Yamamoto, K. Yamamoto, K. Nakahara, N. Kido, Damage of Al_2O_3-MgO-C Brick for Ladle Furnace, Taikabutsu Overseas. 21 (2001) 252–257.

[4] Y. Sasajima, T. Yoshida, S. Hayama, Effect of composition and magnesia particle size in alumina-magnesia-carbon refractories., in: Proc. UNITECR'89, 1989: pp. 586–603.

[5] R.K. Koley, K.A. V. Rao, S. Askar, S.K. Srivastava, Development and application of Al_2O_3-MgO-C refractory for secondary refining ladle, in: Proc. UNITECR'01, 2001.

[6] P. Tassot, F. Etienne, J. Wang, P. Atkinson, New concepts for steel ladle linings, in: Proc. Unified Int. Tech. Conf. Refract. UNITECR'07, 2007: pp. 462–465.

[7] V. Muñoz, P.G. Galliano, E. Brandaleze, A.G. Tomba Martinez, Chemical wear of Al_2O_3-MgO-C bricks by air and basic slag, J. Eur. Ceram. Soc. 35 (2015) 1621–1635. doi:10.1016/j.jeurceramsoc.2014.11.024.

[8] J. Pötsche, T. Deinet, The Corrosion of AMC-Refractories by Steel and Slago Title, in: UNITECR'05, Orlando, 2005: pp. 75–79.

[9] J. Pötsche, T. Deinet, G. Routschka, R. Simmat, Properties and Corrosion of AMC-Refractories (Part 1: Characterization and Oxidation), in: UNITECR'03, 2003: pp. 580–587.

[10] J. Poirier, M. Bouchetou, P. Pringent, J. Berjonneau, an overview of refractory corrosion: observations, mechanisms and thermodynamic modeling, Refract. Appl. Trans. 3 (2007) 2–12.

[11] W.A. Calvo, P. Ortega, M.J. Velasco, V. Muñoz, P. Pena, A.G.T. Martinez, Characterization of alumina-magnesia-carbon refractory bricks containing aluminium and silicon, Ceram. Int.

44 (2018) 8842–8855. doi:10.1016/j.ceramint.2018.02.069.

[12] DIN EN 993-1 (DIN 51056), Method of test for dense shaped refractory products. Determination of bulk density, apparent porosity and true porosity (1995).

[13] G. Urbain, F. Ambier, M. Deletter, M.R. Anseau, Viscosity of silicate melts, Br. Ceram. Soc. 80 (1981) 139–141.

[14] V. Muñoz, S. Camelli, A.G. Tomba Martinez, Slag corrosion of alumina-magnesia-carbon refractory bricks: Experimental data and thermodynamic simulation, Ceram. Int. 43 (2017) 4562–4569. doi:10.1016/j.ceramint.2016.12.114.

[15] A.P. Luz, A.G.T. Martinez, M.A.L. Braulio, V.C. Pandolfelli, Thermodynamic evaluation of spinel containing refractory castables corrosion by secondary metallurgy slag, Ceram. Int. 37 (2011) 1191–1201. doi:10.1016/j.ceramint.2010.11.043.

[16] C. Taffin, J. Poirier, The Behaviour of Metal Additives in MgO-C and Al_2O_3-C Refractories, Interceram. 43 (1994) 354–460.

[17] C. Alvarez, E. Criado, C. Baudin, Refractarios de magnesia-grafito, Bol. Soc. Esp. Ceram. Vidr. 31 (1992) 397–405.

[18] H. Ishii, M. Nagafune, I. Tsuchiya, Y. Oguchi, T. Kawakami, Reaction between Magnesia and Carbon at High Temperature, in: Unitecr'89. Proc. Unified Int. Tech. Conf. Refract., 1989: p. Vol. 2, pp. 1704–1721.

[19] K. Tabata, H. Nishio, K. Itoh, Study on Oxidation-Reduction Reaction in MgO-C Refractories, Taikabutsu Overseas. 8 (1988) 3–10.

[20] I.Z. Yildirim, M. Prezzi, Chemical, mineralogical, and morphological properties of steel slag, Adv. Civ. Eng. 2011 (2011). doi:10.1155/2011/463638.

[21] W. Posch, H. Presslinger, H. Hiebler, Mineralogical evaluation of ladle slags at voestalpine Stahl GmbH, Ironmak. Steelmak. 29 (2002) 308–312. doi:10.1179/030192302225005169.

[22] M.N. Moliné, W.A. Calvo, A.G.T. Martinez, P.G. Galliano, Ambient weathering of steelmaking ladle slags, Ceram. Int. en prensa (2018) 1–8.

doi:10.1016/j.ceramint.2018.07.128.

[23] L.M. Juckes, The volume stability of modern steelmaking slags, Miner. Process. Extr. Metall. (Trans. Inst. Min. Met. C). 112 (2003) 177–197. doi:10.1179/03719550322500370.

[24] J.P. Guha, Reaction Chemistry in Dissolution of Polycrystalline Alumina in Lime–Alumina–Silica Slag, Br. Ceram. Trans. 96 (1997) 234–236.

[25] S. Zhang, H.R. Rezaie, H. Sarpoolaky, W.E. Lee, Alumina Dissolution into Silicate Slag, J. Am. Ceram. Soc. 83 (2000) 897–903. doi:10.1111/j.1151-2916.2000.tb01291.x.

[26] S. Yilmaz, Corrosion of high alumina spinel castables by steel ladle slag, Ironmak. Steelmak. 33 (2006) 151–156. doi:10.1179/174328106X80109.

[27] W.E. Lee, S. Zhang, Melt corrosion of oxide and oxide-carbon refractories, Intenational Mater. Rev. 44 (1999) 77–104.

[28] P. Williams, A. Hagni, Mineralogical studies of alumina magnesia carbon steel ladle refractories, in: UNITECR'97. Proc. Unified Int. Tech. Conf. Refract. 5 Th Bienn. Worldw. Congr. Refract. A Worldw. Technol., 1997: p. Vol. 1, pp. 183–192.

[29] C. Baudín, C. Alvarez, R.E. Moore, Influence of Chemical Reactions in Magnesia – Graphite Refractories : I , Effects on Texture and High-Temperature Mechanical Properties, J. Am. Ceram. Soc. 82 (1999) 3529–3538. doi:https://doi.org/10.1111/j.1151-2916.1999.tb02276.x.

[30] C. Baudín, High temperature mechanical behavior of magnesia-graphite refractories, in: J. Bennett, J.D. Smith (Eds.), Fundam. Refract. Technol., 2006: pp. 73–92. doi:10.1002/9781118370940.ch4.

[31] Y. Kiyota, Reduction of permanent linear change of alumina-magnesia castable, in: Proc. Unified Int. Tech. Conf. Refract., 2007: pp. 546–549.

[32] M.A.L. Braulio, E.W. Zinngrebe, S.R. Van Der Laan, V.C. Pandolfelli, Steel ladle well block post mortem analysis, Ceram. Int. 38 (2012) 1447–1462. doi:10.1016/j.ceramint.2011.09.027.

[33] V. Muñoz, A.G. Tomba Martinez, Thermomechanical behaviour of Al_2O_3-MgO-C refractories under non-oxidizing atmosphere., Ceram. Int. 41 (2015) 3438–3448. doi:10.1016/j.ceramint.2014.10.146.

[34] V. Muñoz, A.G.T. Martinez, Factors controlling the mechanical behavior of alumina-magnesia-carbon refractories in air, Ceram. Int. 42 (2016) 11150–11160. doi:10.1016/j.ceramint.2016.04.021.

Table 1. Characteristics of the unused AMC4 brick.

Composition (wt.%)		**Particles' sizes (μm)**
Corundum (Al_2O_3)	77.7±0.1	< 4670
Periclase (MgO)	6.6±0.1	2000-100
Graphite (C)	1.9±0.1	125-25
Aluminum (Al)	2.8±0.1	10-50
Silicon (Si)	0.4±0.1	
Resin (C, O, H)	4.4±0.1	-
Impurities[(1)]	6.1±0.1	-
Porosity	V_p[(2)] (%)	13
	π_a[(3)] (%)	3.6 ± 0.1
	K_p[(4)] (mD)	< 0.3

[(1)] Fe_2O_3, SiO_2, CaO, TiO_2 [(2)] V_p: volume percentage of pores < 1 μm

[(3)] π_a: apparent porosity [(4)] K_p: permeability

Table 2. Characteristics of analyzed slags.

	Slag	m-slag	a-slag
Composition (wt.%)	CaO	55.7 ± 0.6	51.7 ± 0.6
	Al_2O_3	27.2 ± 0.7	34.8 ± 0.7
	MgO	8.3 ± 0.3	7.2 ± 0.3
	SiO_2	7.7 ± 0.1	4.9 ± 0.1
	FeO	0.53 ± 0.04	0.84 ± 0.04
	S	0.49 ± 0.01	0.38 ± 0.01
	Cr_2O_3	0.030 ± 0.002	0.11 ± 0.002
	MnO	0.070 ± 0.002	0.050 ± 0.002
Basicity [(1)]		1.6	1.3
μ	1300°C	7.84	11.03
(Poise)	1700°C	0.92	1.14

[(1)] $CaO/(SiO_2+Al_2O_3)$, in weight

Table 3. Solid phases in equilibrium in AMC4 at temperatures between 700 and 1700°C.

T	Weight percentage (wt.%)							
	Al_2O_3	**MgO**	**Al**	**Si**	**Graphite**	**Spinel[(1)]**	**Al_4C_3**	**SiC**
RT	87.00	7.40	3.15	0.39	2.15	-	-	-
700°C	68.16	-	-	-	0.94	26.14	4.20	0.55
1000°C	67.96	-	-	-	0.94	26.34	4.20	0.55
1100°C	67.58	-	-	-	0.94	26.72	4.20	0.55
1200°C	66.75	-	-	-	0.94	27.55	4.20	0.55
1400°C	62.27	-	-	-	0.94	32.03	4.20	0.55
1600°C	49.30	-	-	-	0.94	45.00	4.20	0.55
1700°C	36.53	-	-	-	0.94	57.77	4.20	0.55

[(1)] Non stoichiometric

Table 4. Equilibrium phases during cooling of m-slag.

T	Composition (wt.%)					
	Liquid[(1)]	**$Ca_3Al_2O_6$**	**MgO**	**Ca_2SiO_4**	**$CaAl_2O_4$**	**CaO**
1600°C	92.6	0	3.3	0	0	4.1
1450°C	90.2	0	4.6	0	0	5.2
1300°C	24.6	55.5	7.2	12.7	0	0
1150°C	0	68.4	8.2	14.6	8.8	0
1000°C	0	68.0	8.2	14.6	9.2	0

[(1)] Main components: Al_2O_3 and CaO; SiO_2 and MgO < 10 wt.% each one.

Table 5. Crystalline phases in *post-mortem* samples (XRD; ICDD files in parenthesis).

Sample	Corundum	Periclase	Graphite	Al	Si	$MgO \cdot Al_2O_3$	Others
	(11-0661)	(45-0946)	(41-1487)	(04-0787)	(27-1402)	(45-0946)	
PM1	++++	n.d.	++	n.d.	n.d.	++	CA, CA_2, CA_6
PM2	++++	n.d.	++	n.d.	n.d.	++	-
PM3	++++	+	++	n.d.	n.d.	++	-
PM4	++++	+	++	n.d.	n.d.	++	-

Table 6. Mass losses (TGA), density and porosity of unused and *post-mortem* materials.

Sample	$\Delta m^{(1)}$ (wt.%)	ρ_g (g/cm^3)	π_a (%)	π_t (%)	π_c (%)
Unused	3.8	3.33 ± 0.02	3.6 ± 0.1	6.9 ± 0.6	3.3 ± 0.6
PM4	4.9	3.22 ± 0.01	9.3 ± 0.2	12 ± 1	3 ± 2
PM3	4.9	3.16 ± 0.02	11.5 ± 0.1	14 ± 1	2 ± 1
PM2	5.5	3.14 ± 0.02	12.2 ± 0.6	13 ± 2	1 ± 2
PM1	3.9	3.13 ± 0.02	14 ± 1	12 ± 2	0 ± 3

[(1)]Mass loss calculated from TGA curves between 500 and 800°C.

Table 7. Pore size distributions for PLC testing specimens (small pores <10 µm).

Sample	Volume percentage (%)		
	10 µm < D < 5 µm	**5 µm < D < 1 µm**	**D < 1 µm**
Original	0	65.9	34.1
1000°C[(1)]	0	77.5	22.5
1200°C[(1)]	77.3	20.5	2.2
1400°C[(2)]	89.2	6.8	4

[(1)] 3 cycle [(2)]5 cycle

Figure 1. *Post-mortem* collected fragments of AMC4 bricks.

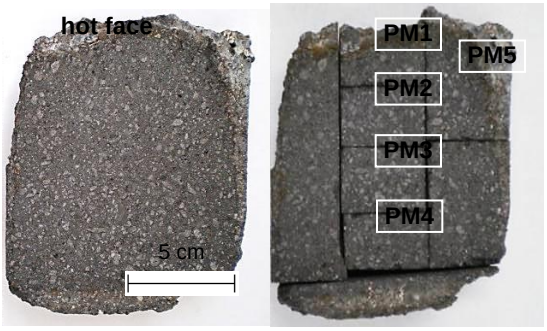

Figure 2. Slices and samples of *post-mortem* AMC4 brick.

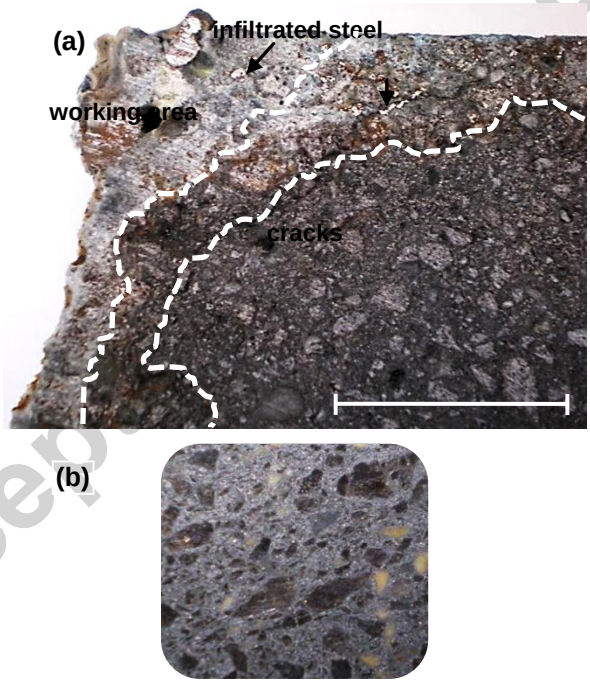

Figure 3. Images of AMC4 bricks: a) *post-mortem* fragment and b) unused.

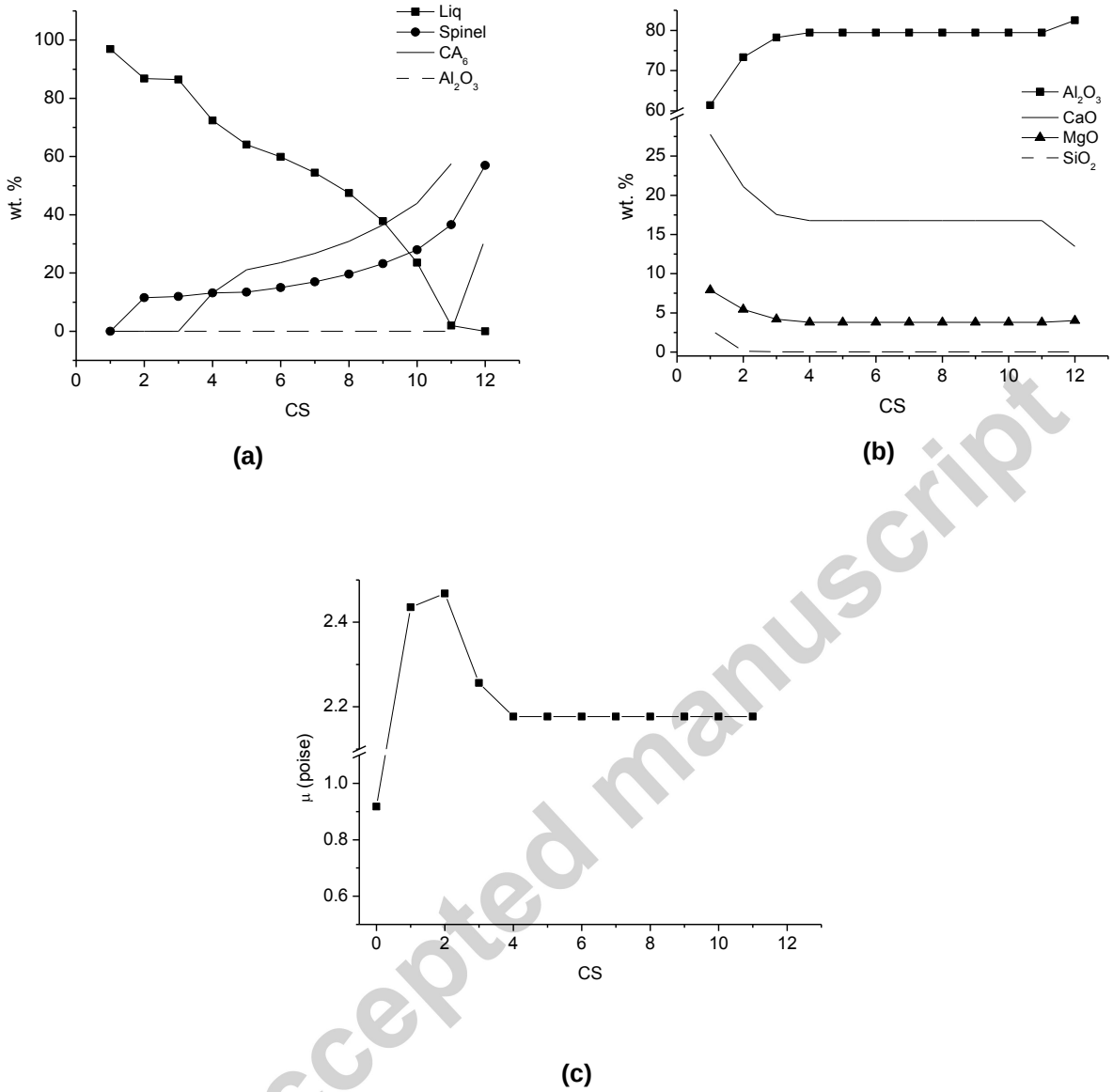

Figure 4. Equilibrium phases in the AMC4-slag system in function of the calculation step (CS): a) proportions (main condensed phases), b) liquid composition and c) liquid viscosity.

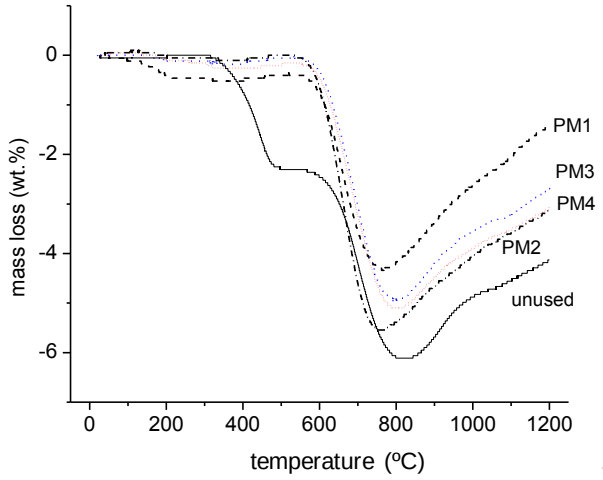

Figure 5. Thermograms (TGA) of unused and *post-mortem* AMC4 materials.

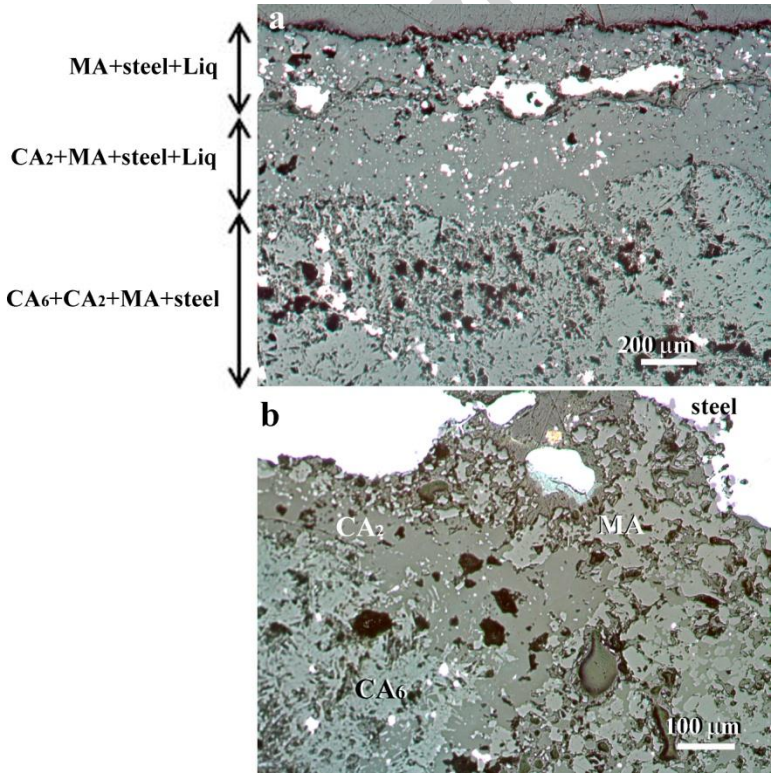

Figure 6. Images of the interface steel+slag/refractory in the *post-mortem* AMC4 brick (RLOM) showing reaction zones.

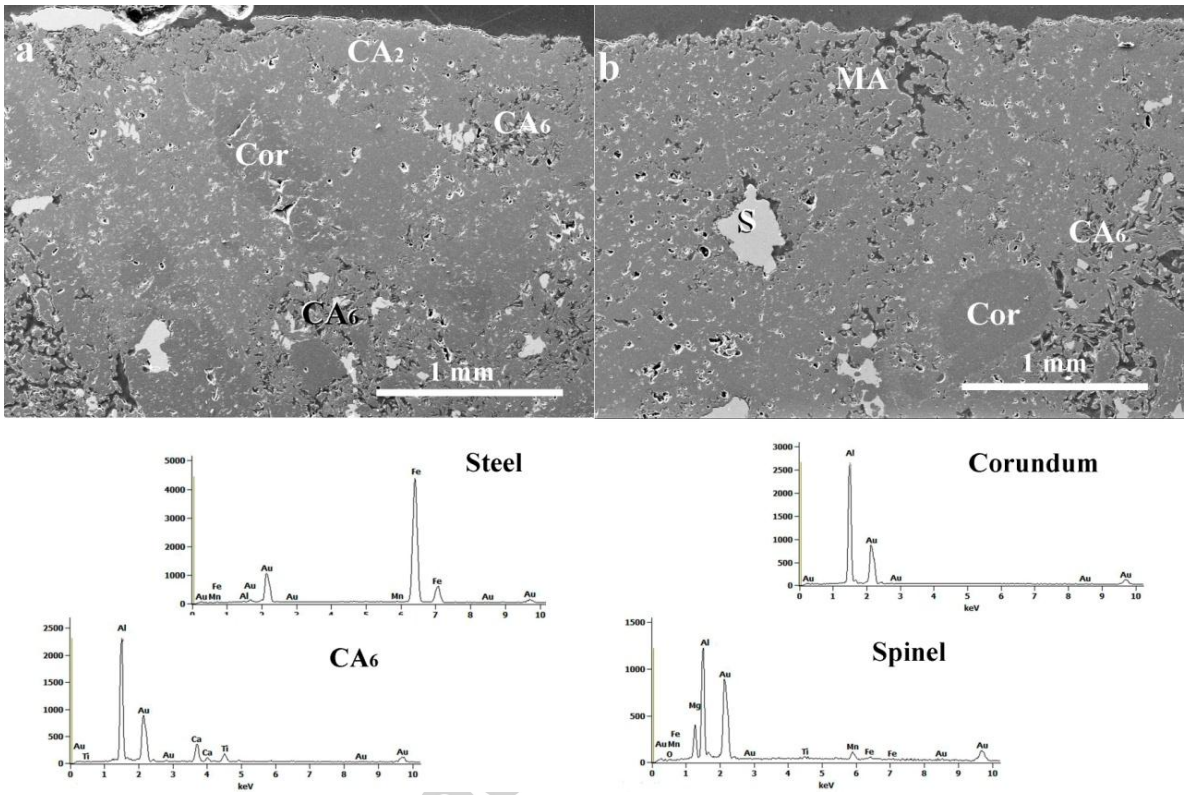

Figure 7: FE-SEM micrographs of two areas of the zone of reaction between slag+steel/AMC4. refractory. The presence of: a) abundant un-reacted corundum grains are clearly observed (Cor); b) steel inclusions (S); c) calcium aluminates (CA_6; CA_2) and d) spinel grains (MA).

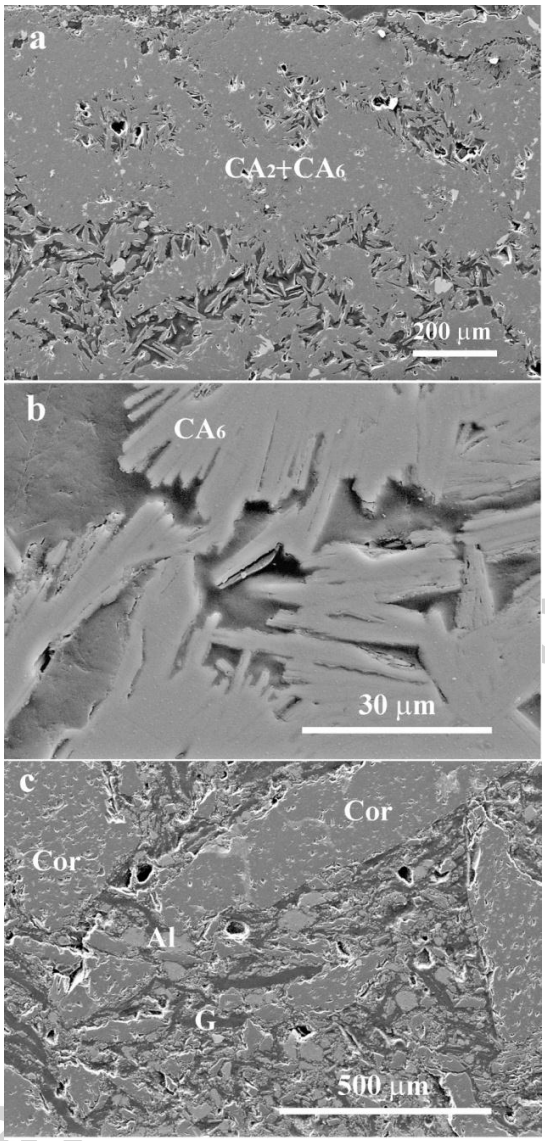

Figure 8: FE-SEM micrographs of the cross section of the slag+steel/AMC4 refractory interface: a) the presence of highly densified areas close to the interface is clearly observed (CA_6; CA_2); b) image showing a detail of the calcium hexaluminate crystals; c) typical microstructure of the uncorroded AMC4 refractory. Cor=Corundum; G=graphite; Al=aluminium.

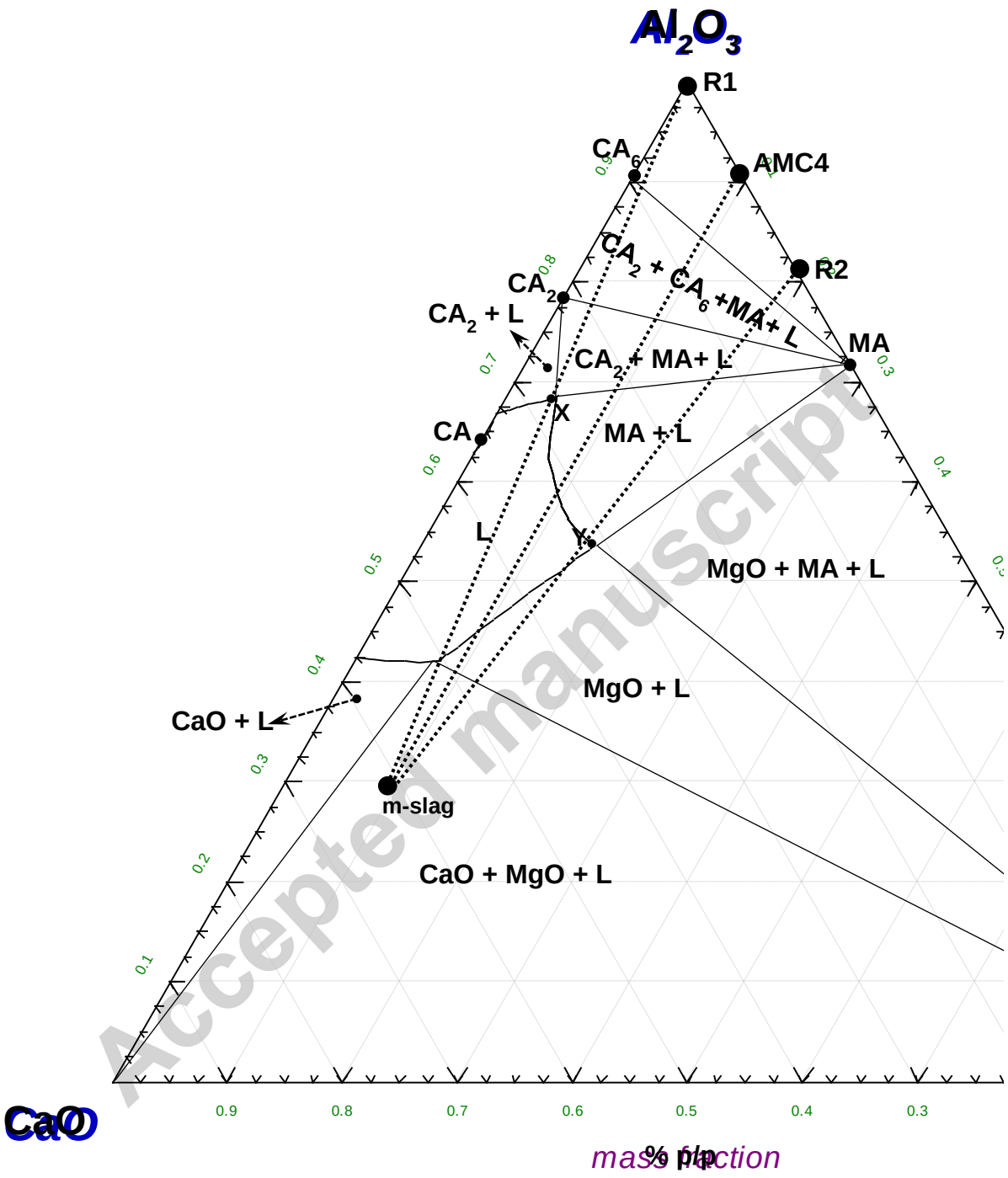

Figure 9. Isothermal section at 16500 ºC of the Al_2O_3-MgO-CaO ternary system showing the reaction path of the calcium aluminate slag against the AMC refractory.

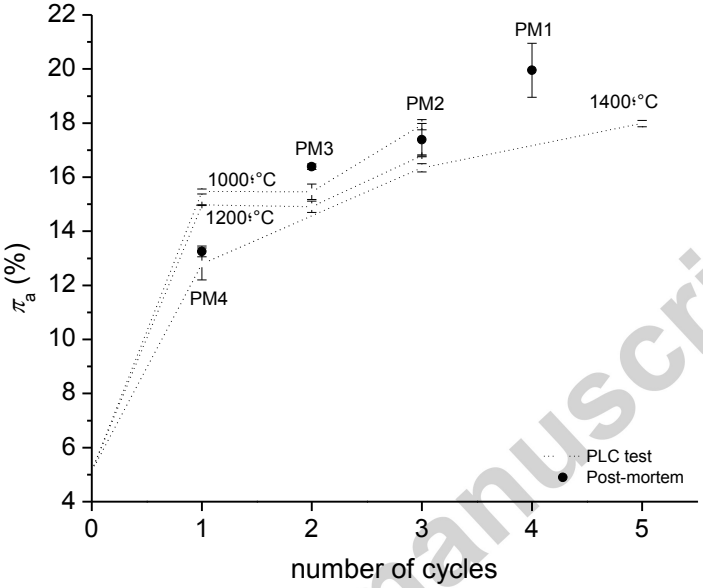

Figure 10. Variation in apparent porosity during PLC testing of AMC4 (in air) and in *post-mortem* samples.